End-chain fluorination of polyesters favors perfluorooctyl bromide encapsulation into echogenic PEGylated nanocapsules

Sophie Houvenagel, Guilherme Picheth, Camille Dejean, Annie Brûlet, Alexis Chennevière, Olivier Couture, Nicolas Huang, Laurence Moine, Nicolas Tsapis

End-chain fluorination of polyesters favors perfluorooctyl bromide encapsulation into echogenic PEGylated nanocapsules

Sophie Houvenagel[a], Guilherme Picheth[a,e], Camille Dejean[b], Annie Brûlet[c], Alexis Chennevière[c], Olivier Couture[d], Nicolas Huang[a], Laurence Moine[a], Nicolas Tsapis[a*]*

[a] *Institut Galien Paris-Sud, CNRS, Univ. Paris-Sud, Université Paris-Saclay, 92296 Châtenay-Malabry, France*

[b] *BioCIS, CNRS, Univ. Paris-Sud, Université Paris-Saclay, 92296 Châtenay-Malabry, France*

[c] *Laboratoire Léon Brillouin, UMR12 CEA-CNRS, CEA Saclay, Gif sur Yvette, F-91191, France*

[d] *Institut Langevin, ESPCI Paris, CNRS (UMR 7587), INSERM (U979), Paris, France*

[e] *Biopol, Chemistry Department, Federal University of Paraná, 81531-980. Curitiba, PR, Brazil*

** Corresponding authors at: CNRS, Institut Galien Paris-Sud, CNRS UMR 8612, Faculté de Pharmacie, 92296 Châtenay-Malabry, France. Tel.: +33 146835813. E-mail address: laurence.moine@u-psud.fr (Laurence Moine) and nicolas.tsapis@u-psud.fr (Nicolas Tsapis).*

Keywords: Perfluorocarbons, nanocapsules, fluorinated polymers, ultrasound contrast agents

Abstract

Perfluorinated end-capped polylactides (PLAs) with various perfluorinated chain lengths from C_3F_7 to $C_{13}F_{27}$ were synthesized and formulated into PEGylated nanocapsules of perfluorooctyl bromide (PFOB) to be used as ultrasound contrast agents (UCAs). We show that the perfluorinated end groups do not reduce the interfacial tension between PFOB and the organic solvent used during formulation and do not allow a significant reduction of shell thickness (Small angle neutron scattering (SANS) experiments). However, PFOB encapsulation efficiency increases with the fluorinated chain length until C_8F_{17}. This suggests the possible presence of favorable fluorophilic interactions between PFOB and perfluorinated end groups. In addition, nanocapsules formulated with the different fluorinated polymers do not promote any specific toxicity *in vitro* compared to non-fluorinated PLAs. Ultrasound imaging performed on samples presenting the lowest thickness values, namely nanocapsules made from 50% PLA-C_6F_{13} / 50% polylactide-*b*-poly(ethylene glycol) (PLA-PEG) and pure PLA-PEG nanocapsules, shows that fluorinated nanocapsules exhibit a higher ultrasound contrast enhancement *in vitro* most probably thanks to the higher PFOB content and density arising from polymer fluorination. This highlights the benefit of fluorination for improving the echogenicity of nano-sized ultrasound contrast agents.

1- Introduction

Ultrasound imaging is an extensively used clinical diagnostic modality which enables safe, cost-effective and non-invasive real-time imaging of tissues. However, the use of ultrasound contrast agents (UCAs) is required to help visualize tissues with similar levels of echogenicity.[1, 2] Commercial UCAs mainly consist of gas microbubbles of 1 – 6 µm stabilized by a layer of lipids or proteins.[3, 4] These UCAs improve the microvasculature visualization, but their use for cancer detection and tumor characterization is limited by their large size and poor stability.[3] Tumor imaging requires more stable nano-sized UCAs which could extravasate into the tumors through leaky endothelium by the enhanced permeation and retention (EPR) effect,[5] provided their half-life in the blood is long enough. Since gas nanobubbles are difficult to stabilize,[6] research has focused on UCAs based on liquid perfluorocarbons which possess low solubility in blood and a difference of acoustic impedance with tissues.[7] To further increase nanosystem stability, several groups have reported the use of polymeric shells which are more resistant to disassembly under ultrasonic waves than lipid or protein layers.[8-15]

In this context, our group has previously developed nanocapsules consisting of a solid polymeric shell of poly(lactide-co-glycolide) (PLGA) and a liquid core of perfluorooctyl bromide (PFOB).[16] PFOB is biocompatible and its liquid state provides good stability and resistance to mechanical stresses and pressure changes. These nanocapsules were previously imaged by ultrasonography in nonlinear mode (Tissue Harmonic Imaging) in the vena cava of a mouse liver after intravenous injection.[17] Nevertheless, due to dilution in the blood and elimination by the mononuclear phagocyte system, these nanocapsules could not allow tumor imaging. PLGA was therefore replaced by poly(lactide-co-glycolide)-poly(ethylene glycol) (PLGA-PEG) copolymer to yield stealth nanocapsules that accumulated in the tumor by the EPR effect (5% of the injected dose), and provided contrast enhancement in tumor with ^{19}F Magnetic Resonance Imaging.[18, 19] Encapsulation of paclitaxel in the PLGA-PEG shell led to a significant twofold reduction in tumor growth as compared with negative control and generic Taxol® group, making these nanocapsules promising for use as theranostic agents.[20] However, their echogenicity further needs to be improved as no ultrasound signal could be detected in tumors. Thinning the shell of plain PLGA/PFOB nanocapsules, by decreasing the amount of polymer used in the formulation, previously enabled to increase their

compressibility and echogenicity *in vitro.*[16, 17] Attempts to use the same strategy with PLGA-PEG resulted in local dewetting of the polymer at the interface between the aqueous phase and PFOB, leading to the formation of PFOB droplets along with nanocapsules instead of yielding nanocapsules with thinner shells.[21]

The aim of this work is therefore to reduce the capsules shell thickness to improve their echogenicity while keeping their stealth properties with PEG chains. Our strategy was to synthesize new perfluorinated end-functionalized polylactide (PLA) polymers and mix them with polylactide-poly(ethylene glycol) (PLA-PEG) to formulate the nanocapsules (Figure 1). We expect the perfluorinated end group to improve the wetting around the PFOB droplet through fluorophilic interactions and promote the formation of capsules with thin shells when we reduce the amount of polymer in the formulation. Indeed, incorporation of perfluoroalkyl chains in a material usually enhances its tendency to self-assemble through the formation of fluorous phases.[22-24]

We therefore synthesized a family of PLAs end-capped with short linear perfluorinated chains of various lengths, from C_3F_7 to $C_{13}F_{27}$, as well as a hydrocarbon control. We present here the characterization of nanocapsules in terms of size distribution, morphology, PFOB encapsulation efficiency, shell thickness by Small Angle Neutron Scattering, cytotoxicity and *in vitro* ultrasound imaging.

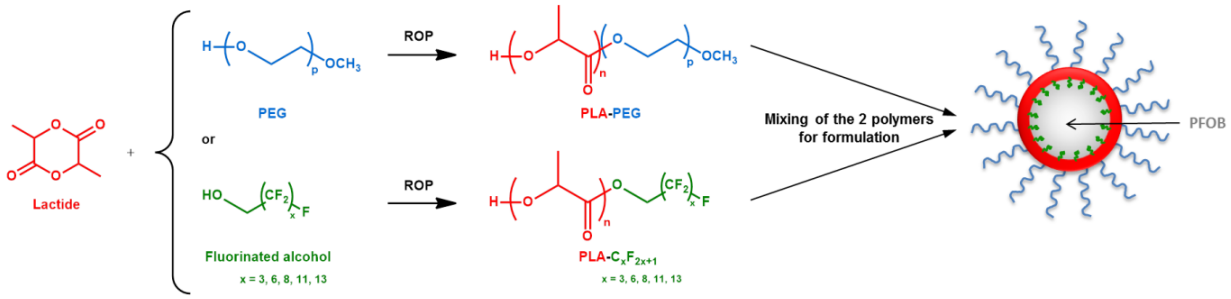

Figure 1: Schematic representation of the strategy used to formulate PEGylated thin nanocapsules

2- Materials and methods

2-1-Materials

DL-lactide was purchased from Biovalley, Polysciences Inc. (USA). Poly(ethylene glycol) methyl ether (OH-PEG-OCH_3, average M_n = 5 000 g/mol), stannous 2-ethyl hexanoate (stannous octoate, $Sn(Oct)_2$), dried toluene, poly(vinyl alcohol) (PVA) (M_w = 30 000-70 000 g/mol, 87-90% hydrolyzed), sodium cholate, D_2O and trifluoroacetic acid (TFA) were provided by Sigma-Aldrich (France). 1-hexanol was from ACROS Organics (Belgium). 2,2,3,3,4,4-heptafluoro-1-butanol, 1H,1H-perfluoro-1-heptanol, 1H,1H-perfluoro-1-nonanol, 1H,1H-perfluoro-1-dodecanol, 1H,1H-perfluoro-1-tetradecanol, perfluorooctyl bromide (PFOB) and perfluoro-1,5-crown-5-ether (PFCE) were purchased from Fluorochem (UK). Deuterated chloroform ($CDCl_3$) and deuterated acetone (acetone-d) were obtained from Euriso-top (France). All solvents were purchased from Carlo Erba (France). Cell culture reagents such as DMEM (Dulbecco's modified Eagle's medium), RPMI 1640 (Roswell Park Memorial Institute medium), FBS (Fetal Bovine Serum), trypsin-EDTA solution and PBS (Ca^{2+} and Mg^{2+} free phosphate buffer) were purchased from Sigma Aldrich (France). Water was purified using a RIOS/Synergy system from Millipore (France). NMR sample tubes and coaxial inserts were obtained from CortecNet (France).

2-2- Polymers synthesis

All polylactide (PLA) derived polymers were synthesized by ring-opening polymerization (ROP) of DL-lactide with the presence of stannous octoate as catalyst.[25, 26] All glassware was dried by heating under vacuum and handled under argon atmosphere. In a 10 mL Schlenck tube equipped with a magnetic stir-bar, the DL-lactide (10.4 mmol, 1.5g) and corresponding initiator (0.075 mmol) – OH-PEG-OCH_3 for polylactide-poly(ethylene glycol) (PLA-PEG), 1-hexanol for PLA-C_6H_{13}, 2,2,3,3,4,4-Heptafluoro-1-butanol for PLA-C_3F_7, 1H,1H-perfluoro-1-heptanol for PLA-C_6F_{13}, 1H,1H-perfluoro-1-nonanol for PLA-C_8F_{17}, 1H,1H-perfluoro-1-dodecanol for PLA-$C_{11}F_{23}$ or 1H,1H-perfluoro-1-tetradecanol for PLA-$C_{13}F_{27}$ – were added to the flask under argon flow. The tube was sealed with a rubber cap and a stannous octoate solution (0.05 mmol, 20 mg) dissolved in 2 mL of dried toluene was added through the septum. The tube was purged with argon for 15 minutes and then placed into a 130°C oil bath. Polymerization was carried out for 55 min under magnetic stirring, and then quenched by immersing the tube in a cold water

bath. After evaporation of toluene, the reaction product was dissolved in chloroform followed by precipitation into excess cold diethyl ether. The product was then dissolved in acetone (or THF for PLA-C_6H_{13} and PLA-PEG) and precipitated into water. The polymer was finally freeze-dried for 24h using an Alpha-1-2 LD apparatus (Christ, France) and a white powder was obtained. Lactide conversion ≥ 95% (^{1}H NMR). ^{1}H NMR (300 MHz, $CDCl_3$, δ, ppm): **PLA-C_6H_{13}, C_3F_7, C_6F_{13}, C_8F_{17}, $C_{11}F_{23}$, $C_{13}F_{27}$**: 5.10-5.28 (C*H*CH_3COO), 4.46-4.81 (OC*H*$_2CF_2$), 4.38 (terminal C*H*CH_3COO), 2.73 (terminal *H*OCHCH_3COO), 1.52-1.61 (CHC*H*$_3$COO); **PLA-PEG:** 5.10-5.28 (C*H*CH_3COO), 3.64 (OC*H*$_2$C*H*$_2$), 1.52-1.61 (CHC*H*$_3$COO). ^{19}F NMR (200 MHz, $CDCl_3$, δ, ppm): **PLA-C_3F_7**: -79.0 (C*F*$_3$), -118.7 (CH_2C*F*$_2$), -125.8 (CF_2C*F*$_2$C*F*$_3$); **PLA-C_6F_{13}, C_8F_{17}, $C_{11}F_{23}$, $C_{13}F_{27}$:** -79.0 (C*F*$_3$), -117.7 (CH_2C*F*$_2$), -120.0 ((CF_2)$_{x-5}$$CF_2CF_3$), -120.8 ($CH_2CF_2$C*F*$_2$), -121.4 ($CH_2CF_2CF_2$C*F*$_2$), -124.3 (C*F*$_2CF_3$).

2-3- Polymers characterization

Size Exclusion Chromatography (SEC) was performed at 30 °C with two columns from Polymer Laboratories (PL-gel MIXED-D; 300 × 7.5 mm) and a differential refractive index detector (Spectrasystem RI-150, Thermo Electron Corp.), using chloroform as an eluent, a Waters 515 pump at a flow rate of 1 mL/min, and toluene as a flow-rate marker. The calibration curve was based on poly(methyl methacrylate) (PMMA) standards from Polymer Laboratories.

^{1}H NMR and ^{19}F NMR spectroscopies were performed in 5 mm diameter tubes in $CDCl_3$ or acetone-d on a Bruker Avance-300 (300 MHz) spectrometer and a Bruker ARX-200 (200 MHz) spectrometer, respectively.

The molar masses of PLA-C_xF_{2x+1} were also estimated by ^{19}F NMR with PFCE as an internal standard on the hypothesis that all polymer chains have the same lengths and all polymer chains have a fluorinated end group. A known mass of fluorinated polymer was dissolved in a precise volume of a solution of PFCE at 0.293 mmol/L in $CDCl_3$. The molar concentration of PLA-C_xF_{2x+1} was calculated by integrating the resonance peak at -78.9 ppm, corresponding to the CF_3 group of PLA-C_xF_{2x+1} and normalized by the area of the single resonance PFCE peak at -87.6 ppm. The molar mass was deduced from the calculated molar concentration and the known mass in the tube.

Differential scanning calorimetry (DSC) was performed using a DSC Q1000 (TA Instruments). The polymers (2-5 mg) were sealed in aluminum pans and heated from 20 to 70°C at a heating rate of 20°C/min and cooled to 20 °C before a second heating scan from 20 to 70°C at 20°C/min to determine the glass transition temperature (T_g). A nitrogen flow was maintained throughout the test (20 mL/min).

2-4- Interfacial tension measurements

The interfacial tension measurements were carried out using the pendant drop method, employing a Tracker tensiometer (Teclis, France). Drops of PFOB of 0.1-0.3 µL were formed using a syringe and a G22 stainless steel needle into a methylene chloride solution containing the polymers at 25 mg/mL placed in an optical glass cuvette. The interfacial tension was determined from the drop profile using the Laplace equation and the forces balance between capillarity and gravity. The measurements were performed on at least three independent drops and the experiment was repeated on different days to ensure reproducibility.

2-5- Nanocapsules preparation

Nanocapsules (NCs) of PFOB were prepared by an emulsion-evaporation process as previously described.[16, 18] PLA-PEG or a mixture of 50 wt% PLA-PEG with 50 wt% PLA-C_6H_{13} or PLA-C_xF_{2x+1} (total mass 30 mg or 50 mg), was dissolved into 2 mL of methylene chloride along with 30 µL of PFOB. The organic phase was emulsified into 10 mL of 1.5 % sodium cholate (w/v) aqueous solution using a vortex for 1 min and then a vibrating metallic tip (Digital Sonifier, Branson Ultrasons, France) at 30% of maximal power, for 1 min over ice. Solvent was allowed to evaporate by magnetic stirring at 300 rpm at room temperature for 3 h. The native suspensions of NCs were filtered through 0.45 µm PVDF filters, and if necessary, were purified to remove sodium cholate by ultracentrifugation for 1h, at 4 °C and at 27 440 g (Optima LE-80K Ultracentrifuge Beckman Coulter). The pellet was finally resuspended in water to the desired concentration.

2-6- Size distribution and Zeta potential

The hydrodynamic diameter (d_H) and polydispersity index (PDI) of the nanocapsules were measured by quasi elastic light scattering, using a Zetasizer Nano ZS instrument (Malvern, France). Suspensions were diluted in water

to a concentration of 1 mg/mL. Measurements were performed at 20 °C, at an angle of 173° to avoid multiple scattering. Zeta potential measurements were carried out with the same instrument, at 25 °C, in 1 mM NaCl. Measurements were performed in triplicate.

2-7- PFOB encapsulation efficiency by ^{19}F NMR spectroscopy

PFOB encapsulation efficiency was determined by ^{19}F NMR on a Bruker Avance-400 (400 MHz) spectrometer with a 5 mm dual probe ^{19}F/^{1}H. The NMR quantitative method using stem coaxial inserts was originally proposed by Henderson for ^{31}P compounds[27] and adapted previously for ^{19}F NMR.[19] 1 mL of unpurified and filtered nanocapsules were freeze-dried for 24h using an Alpha-1-2 LD apparatus (Christ, France) and lyophilisates were dissolved into 1 mL of chloroform. Sodium cholate was removed by centrifugation for 5 min at 4696 g. The organic solution was collected and introduced into a usual 5mm-NMR sample tube loaded with a stem coaxial insert containing TFA in D_20 as an external standard ([TFA]= 9.4 µmol.mL^{-1}). The total amount of PFOB in the suspension, n_{PFOB}, was determined after integration of the peak at -64.7 ppm corresponding to the CF_2Br group and normalization by the area of the TFA peak at -76.5 ppm using a PFOB calibration curve in chloroform (supplementary information). Absolute encapsulation efficiency, η_{encaps}, was calculated as follows:

$$\eta_{encaps} = \frac{n_{PFOB}}{n_{PFOB}^{max}} \text{ with } n_{max} = \frac{m_{PFOB}^{feed}}{M_{PFOB}} \frac{m_{NC}}{m_{PFOB}^{feed} + m_{polymer}^{feed} + m_{SC}^{feed}}$$

where m_{PFOB}^{feed}, $m_{polymer}^{feed}$ and m_{SC}^{feed} are the initial masses of the components introduced during NCs preparation, m_{NC} corresponds to the mass of NCs recovered after freeze-drying and M_{PFOB} is the molar mass of PFOB (498.96 g/mol).

2-8- Transmission electron microscopy (TEM)

TEM was performed at I2BC (Gif-sur-Yvette, France) using a JEOL JEM-1400 operating at 80 kV. 5 µL of purified suspensions of nanocapsules (0.5 mg/mL) were deposited for 1 min on glow-discharged copper grids covered with formvar-carbon film. Samples were then stained using 2% phosphotungstic acid (pH = 7) for 30 s. The excess solution was blotted off using a filter paper. Images were acquired using an Orius camera (Gatan Inc, USA).

2-9- Cryo-transmission electron microscopy (cryo-TEM)

Cryo-TEM was performed at I2BC (Gif-sur-Yvette, France) using a JEOL JEM-1400 operating at 120 kV. 5 µL of purified suspensions of nanocapsules (25 mg/mL) were deposited on glow-discharged Lacey copper grids covered with carbon film containing holes. The excess solution was blotted off for 5 s using filter paper and the grids were subsequently frozen in liquid ethane using a Leica EM GP automatic system (Leica, Austria) under a 90% humidity atmosphere. Images were recorded on a US1000XP camera (Gatan Inc, USA) with a -2 µm defocus.

2-10- Small angle neutrons scattering (SANS)

2-10-1- SANS data collection

Small Angle Neutron Scattering (SANS) measurements were performed on the PACE and TPA spectrometers of the Laboratoire Léon Brillouin (LLB, CEA-Saclay, France). Nanocapsules were filtered, purified and resuspended in the desired mixture of H_2O and D_2O at a final volume fraction of ϕ_v = 1%. Two mixtures were used to match or not the scattering length densities of the various components, PFOB or PLA, and to focus on the structure of the selected features. In water, we expected core-shell structures with PFOB as core and the mixture of PLA-based polymers as shell. The 40/60 (v/v) H_2O/D_2O mixture matched the scattering length density of the PFOB core ($\rho_{PFOB} = \rho_{core}$ = 3.6 x 10^{10} cm^{-2}) and enabled to focus on the polymeric shell. The 67/33 (v/v) H_2O/D_2O mixture matched the scattering length density of PLA ($\rho_{PLA} = \rho_{shell}$ = 1.7 x 10^{10} cm^{-2}) and allowed observing the PFOB core. Two configurations were used on PACE: the first one with a sample-to-detector distance of D = 2.9 m and a neutron wavelength of λ = 4.6 Å to cover a scattering vector (q) range of 3.2 × 10^{-3} – 3.4 × 10^{-2} $Å^{-1}$; the second one with D = 4.7 m and λ = 13 Å to cover a q range of 1.4 × 10^{-2} – 1.5 × 10^{-1} $Å^{-1}$. Samples in PLA matching condition were further analyzed with the TPA spectrometer, the Very SANS (VSANS) spectrometer at LLB. This high resolution VSANS spectrometer with a sample-to-detector distance of D = 6 m and a neutron wavelength of λ = 6 Å allowed to cover a q range of 5.6 x 10^{-4} – 4.0 x 10^{-3} $Å^{-1}$. SANS and VSANS measurements were performed in 1 mm thick quartz cuvettes to minimize the incoherent scattering. Scattered intensity curves were corrected from the scattering from the empty quartz cuvette and the electronic background, and normalized (only for SANS

measurements, not VSANS ones) by the incoherent signal of 1 mm water sample to account for non-uniform efficiency of detector , using the LLB PASINET software.[28]

2-10-2- SANS data modelling

Vesicle model

The scattered intensity curves obtained in PFOB matching condition were fitted using the vesicle model with Sasview software.[29] This model provides the form factor, P(q), for a unilamellar vesicle of inner radius R_{core} and thickness T, according to the following equation:

$$P(q) = \frac{scale}{V_{shell}}\left[\frac{3V_1(\rho_1 - \rho_2)\,J_1(qR_1)}{qR_1} + \frac{3V_2(\rho_2 - \rho_{solv})\,J_1(qR_2)}{qR_2}\right]^2$$

Where scale is a scale factor, V_{shell} is the volume of the shell, V_1 is the volume of the core, V_2 is the total volume of the vesicle, $R_1 = R_{core}$ is the radius of the core, R_2 is the outer radius of the vesicle ($R_2 = R_{core}$ + T). For the vesicle, $\rho_1 = \rho_{core} = \rho_{solv}$ is the scattering length density of the core and the solvent, $\rho_2 = \rho_{shell}$ is the scattering length density of the shell, and $J_1(x) = \frac{\sin x - x\cos x}{x^2}$. The fit gives geometrical parameters of the nanocapsules: the mean core radius R_{core}, the polydispersity of the core radius σ_{core}, the thickness of the shell T and the polydispersity of the thickness σ_T. A lognormal distribution was assumed for both radius and thickness.

Guinier regime

In PLA matching condition, the scattering intensity corresponds to the fluctuations of the PFOB core. The scattered intensity curves in this matching condition were fitted at low q values ($q < 2.5\ 10^{-3}$ Å^{-1}) to determine the radius of gyration R_g using the Guinier approximation with Sasview software according to:

$$I(q) = I_0 \exp\left(-\frac{q^2 R_g^2}{3}\right) \qquad qR_g < 1$$

For a sphere, the radius of gyration is related to the radius of the sphere with the formula:

$${R_{sphere}}^2 = 5/3\,{R_g}^2$$

2-11- Cell culture and cell viability studies

The cytotoxicity of all NCs was evaluated in two distinct cell lines obtained from ATCC (USA). Human endothelial umbilical vein cells (HUVEC) were cultured in DMEM supplemented with 50 $U.mL^{-1}$ penicillin, 50 $U.mL^{-1}$ streptomycin, and 10% heat inactivated FBS. The J774.A1 murine macrophage– monocyte cell line was cultured in RPMI 1640 medium supplemented with 50 $U.mL^{-1}$ penicillin, 50 $U.mL^{-1}$ streptomycin, and 10% heat inactivated FBS. Cells were split twice a week, by trypsinisation for HUVEC and by scraping for J774.A1 cells. All cell lines were maintained at 37 °C and 5% CO_2 in a humidified atmosphere. In order to evaluate the *in vitro* cytotoxicity, NCs were resuspended in cell culture medium before being added onto the cells. The cell viability was evaluated using the 3-[4,5-dimethylthiazol-2-yl]-3,5-diphenyltetrazolium bromide (MTT) assay. Briefly, cells were seeded in 100 µL of culture medium (12 x 10^3 cells/well or 3 x 10^3 cells/well for 24 and 72 h incubation respectively) in 96 well plates (TPP, Switzerland) and pre-incubated for 24 h. 100 µL of a serial dilution of NCs (0.01 to 10 mg/mL) was then added to the medium. After 24 or 72h of incubation, the incubation medium was replaced by fresh medium containing 0.5 mg/mL of MTT (Sigma, France). After 1h15 incubation, the culture medium was gently aspirated and replaced by 200 µL dimethylsulfoxide (ACS grade, VWR, France) to dissolve the formazan crystals. The absorbance of the solubilized dye, which correlates with the number of living cells, was measured with a microplate reader (LAB Systems Original Multiscan MS, Finland) at 570 nm. The percentage of viable cells in each well was calculated as the absorbance ratio between NC–treated and untreated control cells.

2-12- *In vitro* ultrasound imaging

In vitro ultrasound imaging experiments were performed using a programmable ultrasound scanner with a 5 MHz probe with 192 elements. 0.8 mL of purified nanocapsules resuspended at a final concentration of 50 mg/mL were placed in a silicone tube in a 37°C thermostated bath. A picture of the set-up is given in supplementary material (Figure S8). Images were obtained using an ultrafast B-mode sequence[30] at X0.1 MPa peak negative pressure. Ultrafast images were acquired at a frame rate of 100 Hz and data were transferred to a computer for analysis by Matlab (Mathworks, Natick, MA, USA). The backscattered intensity of the samples was obtained by averaging the power of the first and last image of the video in the region-of-interest (the silicone tube). The

resulting intensities were subtracted by the backscattered intensity obtained with the tube filled with Milli-Q water. Commercial Sonovue microbubbles (diluted to 1/1000) were used as a reference positive control for the ultrasound set-up and parameters chosen for our study.

3- Results and discussion

3-1- Polymers synthesis and characterization

Polylactide polymers terminated by a perfluorinated end chain of increasing length (C_xF_{2x+1} with x = 3, 6, 8, 11, 13) were synthesized by ring opening polymerization (ROP) of lactide initiated by fluorinated alcohols of respective lengths. A control terminated by a hydrogenated chain (PLA-C_6H_{13}) and polylactide-*b*-poly(ethylene glycol) (PLA-PEG) were also synthesized by ROP of lactide initiated respectively by hexyl alcohol and polyethylene glycol methyl ether of 5,000 g/mol. The same monomer/initiator feed molar ratio of 278 was used for all polymers to target a 20,000 g/mol PLA block, which allows studying the influence of the end group alone.

Preliminary tests targeting a polymerization degree of 20 were performed to verify by ^{1}H NMR the ability of fluorinated alcohols to initiate the polymerization of lactide. As shown in Figure 2, the triplet at 4.10 ppm corresponding to the CH_2 of the initiator is shifted to 4.65 ppm in the polymer, which confirms the formation of the ester bond and the good initiation by the fluorinated alcohol. Moreover, the ratio of the integral values $2I_{CH_{PLA}}/I_{OCH_2CF_2}$ is approximately 20, which is consistent with the targeted polymerization degree and therefore indicates that within experimental error all polymer chains contain a fluorinated end group. ^{1}H NMR spectra of all synthesized polymers and initiators are shown in supplementary material (Figure S1 and Figure S2).

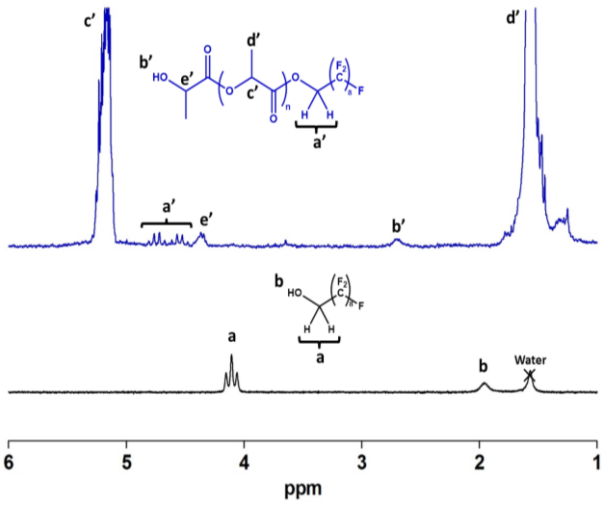

Figure 2: ^{1}H NMR spectrum of a short PLA-C_8F_{17} with 20 lactide units (blue line) and of the fluorinated alcohol (black line) confirming the good initiation of the ROP of lactide by the fluorinated alcohol: shift from 4.10 ppm (H^a) to 4.65 ppm ($H^{a'}$)

^{19}F NMR spectra of all synthesized fluorinated end-capped polymers also present some differences in the CF_2 zone compared to the spectra of their corresponding fluorinated initiators (Figure 3 and Figure S3), confirming again the successful initiation by the fluorinated alcohols.

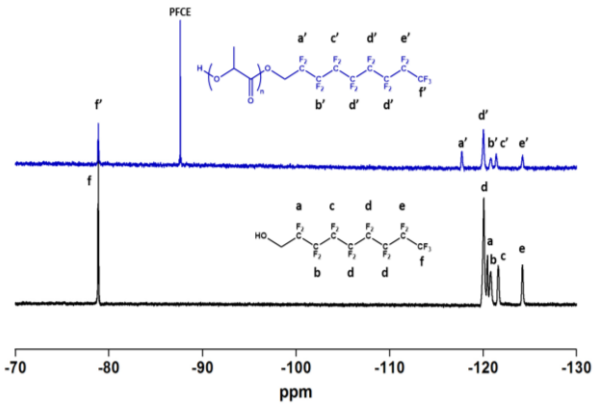

Figure 3: ^{19}F NMR spectra of PLA-C_8F_{17} in $CDCl_3$ with PFCE as internal standard (blue line) and its corresponding fluorinated initiator in $CDCl_3$ (black line)

Molar masses of all synthesized polymers were estimated by SEC and NMR (^{19}F NMR for fluorinated end-capped PLAs and ^{1}H NMR for PLA-PEG) (Table 1). The differences between SEC and NMR values can arise from the difference of conformation of PLA-based polymers in $CHCl_3$ compared to PMMA standards, as well as from the calculation with ^{19}F NMR spectra which is based on the hypothesis that all polymer chains possess a fluorinated end group and have the same length. Both techniques yield M_n values close to the targeted M_n of 20,000 g/mol. Dispersities ($Đ$) are all below 1.5, showing the efficacy of all fluorinated alcohols to initiate the lactide polymerization by ROP (Table 1).

Table 1: Number-average molar mass, dispersity, glass transition temperature of the synthesized polymers, and interfacial tension measured with the pendant drop method at the interface between PFOB and methylene chloride solutions of polymer at 25 mg/mL. Interfacial tension without any polymer is 2.0 ± 0.3 mN/m.

Polymer	M_n^{NMR} (x 10^3 g.mol^{-1})	M_n^{SEC} (x 10^3 g.mol^{-1})	$Đ$	T_g (°C)	Interfacial tension (± 0.3 mN/m)
PLA-PEG	23.5	20.2	1.3	13	2.0
PLA-C_6H_{13}	-	20.8	1.5	52	1.9
PLA-C_3F_7	17.5	23.2	1.5	53	1.7
PLA-C_6F_{13}	17.0	23.5	1.5	51	1.7
PLA-C_8F_{17}	15.5	24.1	1.5	53	2.2
PLA-$C_{11}F_{23}$	16.5	21.9	1.4	53	1.8
PLA-$C_{13}F_{27}$	15.0	21.9	1.5	53	2.2

Glass transition temperatures (T_g) of PLA-C_6H_{13} and all perfluooroalkyl end-capped PLAs are between 51 and 53 °C (Table 1), close to values reported for unmodified PLA polymers.[31-35] Comparatively, Giuntoli et al. observed a decrease of 10-15 °C in the T_g of PLA with incorporation of a C_6F_{13} end chain. This decrease was stronger as the molar mass decreases, however, the molar masses were all lower (5,000 – 12,000 g/mol) than in our study.[36] Indeed, Lee et al. reported a decrease of the T_g of L-PLA from 51 to 34°C upon addition of a $C_{10}F_{21}$ fluorinated end chain at low molar mass (M_n^{SEC} = 14,000 g/mol), but no influence at higher molar mass (M_n^{SEC} = 29,000 g/mol).[25] Considering our results, we assume that 20,000 g/mol is high enough not to observe any influence of fluorinated end chains from C_3F_7 to $C_{13}F_{27}$ on the glass transition of PLA. Regarding PLA-PEG, T_g is strongly reduced to 13 °C, which can be explained by the plasticizing effect of PEG chains,[32] in agreement with previous reports.[37, 38]

3-2- Polymers interfacial properties

Perfluorinated chains are well known to be both hydrophobic and lipophobic, therefore often referred as fluorophilic. Incorporation of perfluoroalkyl moieties in a material usually modifies its surface properties and enhances its propension to self-associate and generate fluorous compartments.[22-24] Our strategy was to favor fluorophilic interactions between PFOB and the perfluorinated end groups of the synthesized polymers, and thus improve the wetting of the polymer layer at the PFOB/aqueous phase interface to yield nanocapsules with thin shells.

The interfacial tension at the PFOB/methylene chloride interface is, however, not modified upon addition of PLA-C_xF_{2x+1} polymers at 25 mg/mL in the methylene chloride phase (Table 1). Values between 1.7 and 2.2 mN/m were

measured for all polymers including the non-fluorinated controls as well as without any polymer, indicating an absence of any interaction between the perfluorinated end chain and PFOB independently of the chain length. The polymers may adopt a certain conformation in the solvent, which would hide the fluorinated groups. This could occur either within a single polymer coil or between several polymer chains, especially if the perfluorinated end chains interact preferentially with each other rather than with PFOB, forming micelles with fluorophilic cores. In the latter case, reducing the polymer concentration should lower these interactions and make the fluorinated groups more accessible for interaction with PFOB. However, attempts to decrease polymer concentration down to 0.1 mg/mL did not induce any change in the interfacial tension. Moreover, no micelles could be detected using DLS analysis of the polymers in methylene chloride. The most probable explanation could be that the proportion of perfluorinated end group compared to the 20,000 g/mol PLA block is not high enough to induce a decrease of the interfacial tension.

3-3- PFOB nanocapsules: physical characterization

Size distribution and zeta potential

For formulation, PLA-PEG was blended with each PLA-C_xF_{2x+1} or PLA-C_6H_{13} (control) at a 50:50 (w/w) ratio in the organic phase to form nanocapsules with a liquid core of PFOB by an emulsion-evaporation process.[16, 18] During the evaporation, we expect the hydrophobic PLA blocks of each polymer to blend homogeneously, the perfluorinated end groups to orientate towards the PFOB core, whereas the hydrophilic PEG chains would orientate towards the aqueous phase (Figure 1). A control formulation with 100% PLA-PEG was also prepared. Since the objective of this study is to reduce shell thickness, we tried to lower the initial mass of polymer in the organic phase (from 50 to 30 mg), while keeping the amount of PFOB constant.

Within experimental error, no significant differences in size can be observed between all samples, which present hydrodynamic diameters in the 110-140 nm range (Table 2). However, polydispersity (PDI) values are higher for formulations prepared from 30 mg of polymer (≥ 0.22) compared to those from 50 mg of polymer (≤ 0.19), suggesting a wider distribution of sizes and eventually the presence of non-encapsulated PFOB droplets as

previously observed with PLGA-PEG,[21] regardless of the polymer used. All samples present negative zeta potential ranging from -24 to -35 mV regardless of the fluorinated chain length (Table 2).

Table 2: Characterization of nanocapsules prepared from total polymer masses of 50 or 30 mg. Data are presented as the mean ± SD (n=3)

	50 mg			30 mg		
Polymer	**d_H (nm)**	**PDI (± 0.02)**	**ζ (mV)**	**d_H (nm)**	**PDI (± 0.02)**	**ζ (mV)**
100% PLA-PEG	113 ± 3	0.18	-24 ± 8	115 ± 4	0.22	-30 ± 9
50% PLA-C_6H_{13} 50% PLA-PEG	125 ± 12	0.18	-25 ± 9	108 ± 6	0.24	-35 ± 9
50% PLA-C_3F_7 50% PLA-PEG	129 ± 13	0.19	-24 ± 9	110 ± 5	0.23	-34 ± 9
50% PLA-C_6F_{13} 50% PLA-PEG	127 ± 12	0.19	-26 ± 12	124 ± 14	0.24	-35 ± 9
50% PLA-C_8F_{17} 50% PLA-PEG	129 ± 13	0.19	-25 ± 8	118 ± 11	0.24	-31 ± 9
50% PLA-$C_{11}F_{23}$ 50% PLA-PEG	137 ± 12	0.18	-29 ± 9	118 ± 10	0.25	-34 ± 7
50% PLA-$C_{13}F_{27}$ 50% PLA-PEG	131 ± 14	0.19	-28 ± 11	111 ± 10	0.24	-34 ± 8

Imaging of nanocapsules

Imaging of nanocapsules by Transmission Electron Microscopy (TEM) and Cryo-Transmission Electron Microscopy (cryo-TEM) revealed no morphological differences related to polymer end-group chemistry, perfluoroalkyl chain length, or polymer quantity. Typical images of nanocapsules made from 50% PLA-C_8F_{17} and 50% PLA-PEG at 50 mg are presented in Figure 4 and supplementary data (Figure S4 and Figure S5). TEM with negative staining shows spherical nanoparticles, with a size and polydispersity in agreement with DLS measurements. Cryo-TEM allows confirming their well-defined core-shell structure. The PFOB core, with high electronic density, appears black and is centered inside the lighter polymeric shell. Nanocapsules also present a white meniscus inside the core. Indeed, rapid freezing of nanocapsules during sample preparation causes solidification and shrinking of PFOB, which does not fill entirely the polymeric shell cavity anymore.[21] Despite the presence of a perfluoroalkyl end group, shell thickness appears polydisperse within a same sample (Figure 4), as previously observed with PLGA-PEG,[21] and unlike plain PLGA nanocapsules.[16]

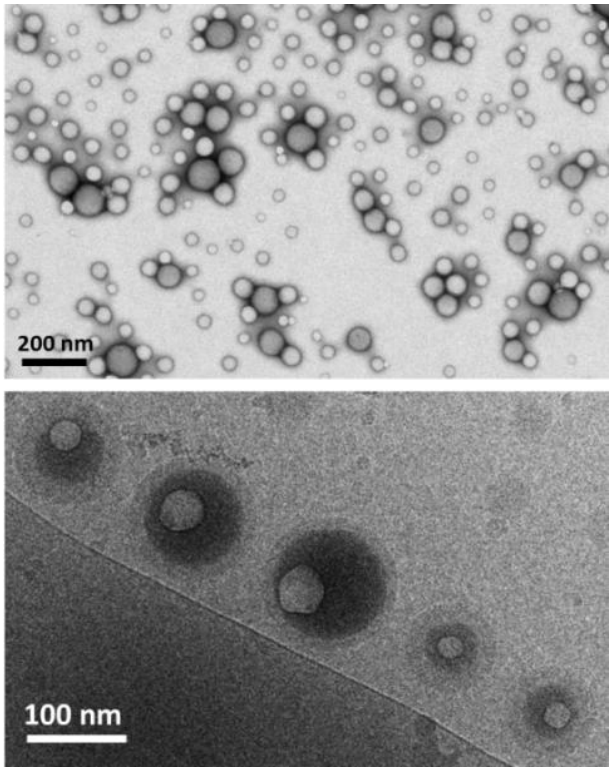

Figure 4: Typical images of nanocapsules made from 50% PLA-C_8F_{17} 50% PLA-PEG (total polymer mass 50 mg) obtained by TEM after negative staining (top) and cryo-TEM (bottom)

PFOB encapsulation efficiency

PFOB encapsulation efficiency in nanocapsules was then measured after freeze-drying to remove any remaining non-encapsulated PFOB droplets. In a general manner, formulations prepared from higher polymer quantity present higher PFOB encapsulation efficiency (59 – 94%) than those obtained with 30 mg polymer (35 – 60%) (Figure 5). This result suggests that 30 mg of polymer might not be sufficient to engulf all the PFOB into nanocapsules (less than 60%).

At high polymer amount, more PFOB is encapsulated in the nanocapsules made from mixtures with 50% PLA-PEG (74-94%) compared to pure PLA-PEG (59%). Although no significant difference can be observed between the non-fluorinated PLA-C_6H_{13} and the fluorinated PLAs, the two highest amounts of encapsulated PFOB are reached with PLA-C_8F_{17} (91%) and PLA-$C_{11}F_{23}$ (94%). This could indicate the presence of favorable fluorophilic interactions between PFOB and the perfluoroalkyl end chains, which might be stronger with increasing fluorinated chain length until a certain point. Indeed, the longest perfluoroalkyl end group leads to a lower PFOB encapsulation

efficiency (74%). This might arise from stronger fluorous interactions between the longest perfluorinated end chains than between PFOB and the perfluorinated end groups, leading eventually to a higher proportion of nanoparticles rather than nanocapsules. Another possible explanation could be that steric hindrance between the fluorines[39] prevents their orientation towards the PFOB core to allow entrapping more PFOB.

At low polymer quantity, the encapsulation efficiency increases with the length of the perfluorinated end group until PLA-C_8F_{17}, suggesting again the presence of favorable fluorophilic interactions between PFOB and the fluorinated end chains. Even though the fluorinated end group did not have an impact on the interfacial tension, it appears to play a role during nanocapsule formulation process, when mixed with 50% PLA-PEG. Such finding is consistent with reports showing successful use of fluorinated polymers to enhance the encapsulation efficiency of fluorinated molecules. Li et al. showed that functionalizing a methoxy-poly(ethylene glycol)-*b*-poly(ε-caprolactone) with a C_3F_7 end chain (mPEG-PCL-C_3F_7) allowed increasing the encapsulation efficiencies of perfluorohexane in nanocapsules from 4.3 to 14.7%.[40] In our case, due to its higher boiling point, PFOB is easier to encapsulate. Still, the end-functionalization with short perfluoroalkyl chains can improve its encapsulation efficiency. The 3-fold increase in encapsulation efficiency observed by Li et al. probably arises from the lower molar mass (PEG 2,000 g/mol and PCL 10,000 g/mol) than in our study, implying a higher proportion of fluorinated end groups therefore promoting stronger fluorous interactions and better encapsulation. The increase of encapsulation efficiency with fluorinated chain length was also observed by Koda et al., though for a very different system.[41]

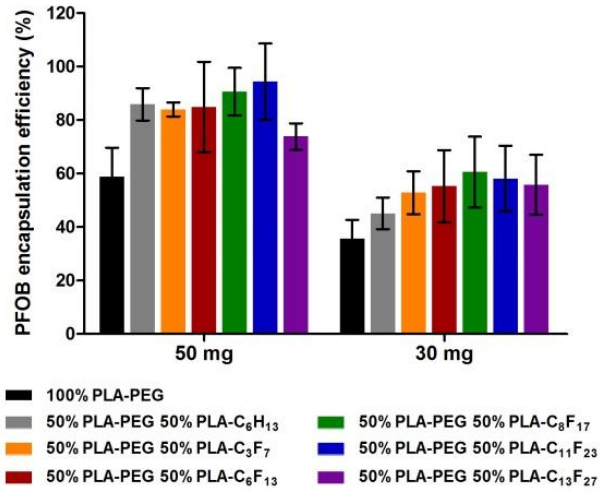

Figure 5: PFOB encapsulation efficiency in freeze-dried nanocapsules. Results are presented as mean ± SD (n = 4)

Morphological features (thickness and core radius) of nanocapsules

Although capsules radii and shell thickness can be measured on cryo-TEM images, the number of imaged capsules is very limited. Small Angle Neutron Scattering (SANS) was therefore used to yield average geometrical parameters on a statistically significant number of nanocapsules. Two contrast matching conditions were used to focus either on the polymer shell or the PFOB core of the capsules.

In PLA matching condition, the scattering curves correspond to the fluctuations of the PFOB core. These curves displayed a q^{-4} variation indicating the presence of sharp interfaces between the PFOB core and the PLA shell. As nanocapsule sizes are large compared to the usual length scales probed with SANS measurements (0.5 – 50 nm), additional experiments were performed at very small angle on the high resolution TPA spectrometer to determine the radius of gyration R_g of the objects. Indeed, in the Guinier range ($q.R_g < 1$), the evolution of scattered intensity follows the equation $I(q) = I_0 \exp\left(-\frac{q^2 {R_g}^2}{3}\right)$, allowing the determination of R_g. Very small angle measurements were performed only with samples in PLA matching condition because the polymer shell of capsules in PFOB matching condition did not scatter enough at very low q. One example of a satisfying fit with this Guinier approximation is given in Figure 6a while others are shown in supplementary material (Figure S7). R_g values of the PFOB core are displayed in Table 3. Since the PFOB core is a sphere as confirmed by microscopy images (Figure 4), the radius of the PFOB core was calculated as ${R_{core}}^2 = 5/3\,{R_g}^2$. Surprisingly, the core radii are

very large (between 110 and 200 nm) and not consistent with both DLS results (hydrodynamic radii of the whole capsules around 55 – 70 nm, Table 2) and cryo-TEM images (PFOB core radii from 30 to 80 nm, Figure 4). We assume that this arises from the presence of some non-encapsulated PFOB droplets which are much larger than the capsules as they tend to coalesce, and are not as visible in DLS since PFOB refractive index is close to the one of water.[42] Although we did not observe any PFOB droplets in cryo-TEM images for these samples, they had been observed previously with PLGA-PEG nanocapsules, with very large sizes and polydispersity.[21]

Table 3: R_g values of the PFOB core obtained from fits with Guinier approximation in PLA matching condition and calculated R_{core} values of the PFOB core with the formula $(5/3)^{1/2}R_g$

Polymer	50 mg		30 mg	
	R_g (nm)	R_{core} (nm)	R_g (nm)	R_{core} (nm)
100% PLA-PEG	101 ± 12	130	86 ± 6	112
50% PLA-C_6H_{13} 50% PLA-PEG	123 ± 5	159	149 ± 4	192
50% PLA-C_3F_7 50% PLA-PEG	117 ± 4	151	124 ± 6	161
50% PLA-C_6F_{13} 50% PLA-PEG	115 ± 1	148	131 ± 5	170
50% PLA-C_8F_{17} 50% PLA-PEG	116 ± 1	150	124 ± 1	160
50% PLA-$C_{13}F_{27}$ 50% PLA-PEG	105 ± 14	135	153 ± 7	198

Except for the 100% PLA-PEG sample, the PFOB radius is larger when the polymer quantity is lowered: 160 – 200 nm for 30 mg compared to 130 – 160 nm for 50 mg (Table 3). This finding is in agreement with the reduced PFOB encapsulation efficiencies at 30 mg (Figure 5), implying a higher proportion of non-encapsulated large PFOB droplets that increase the measured average PFOB radius in SANS. However, this trend is not confirmed with the capsules made from 100% PLA-PEG, which exhibit the lowest radii (130 nm at 50 mg, 112 nm at 30 mg) whereas they present low PFOB encapsulation efficiencies (Figure 5). One reason could be that the capsules made from 100% PLA-PEG are less resistant to the freeze-drying process used to measure the encapsulated PFOB content, whereas the capsules were not freeze-dried for SANS measurements. Indeed, De Jaeghere et al. reported that introduction of PEG to PLA nanoparticles induced their aggregation after freeze-drying. This aggregation was attributed to the tendency of PEG chains to crystallize during the freezing process, this phenomenon being PEG-concentration dependent.[43] In our study, some 100% PLA-PEG capsules might break during freezing and lose their

encapsulated PFOB during the drying process while fluorinated nanocapsules containing less PEG might be stronger.

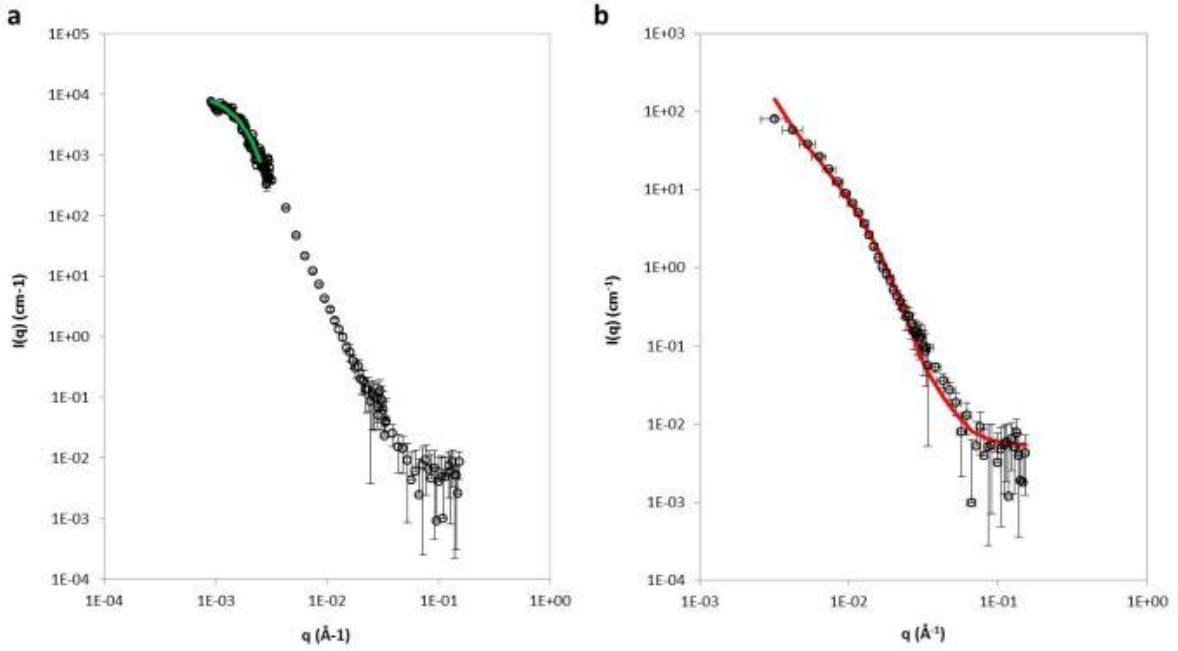

Figure 6: Experimental scattered intensity curves (black circles) of nanocapsules made from 50 mg of 50% PLA-C_6F_{13} 50% PLA-PEG in (a) PLA contrast matching condition fitted with the Guinier approximation at q < 0.0025 $Å^{-1}$ (green line) and in (b) PFOB matching condition fitted with the vesicle model (red line)

Our results in PLA matching condition therefore demonstrated the presence of large non-encapsulated PFOB droplets. PFOB contrast matching was then used to focus on the polymer shell. The scattering curves were fitted with the vesicle model, assuming a lognormal distribution for both thickness and core radius. One example of a satisfying fit is given in Figure 6b while others are shown in supplementary material (Figure S6).

The best fit parameters for all nanocapsules are displayed in Table 4. The mean PFOB core radius values are all in the same range (53 - 57 nm) with a high polydispersity, in agreement with TEM and cryo-TEM images (Figure 4). Core radii are much lower in PFOB matching condition compared to PLA matching condition, confirming that nanocapsules are smaller than non-encapsulated PFOB droplets. Thickness values are also similar for all samples (14.2 - 18.6 nm) and consistent with cryo-TEM images. For all polymers, the mean thickness is slightly reduced when the polymer amount is decreased, although the differences (1 - 4 nm) are not significant. At low polymer quantity, the formulation made from 50% PLA-C_6F_{13} 50% PLA-PEG presents the smallest thickness (14.2 nm) but the one made from 100% PLA-PEG is already very low (14.4 nm). We show here that it is not possible to

significantly decrease the capsules shell thickness with these mixtures of polymers, as previously observed with PLGA-PEG.[21]

Table 4: Geometrical parameters (thickness T and core radius R_{core}) of nanocapsules obtained by SANS curves fitting with the vesicle model

Polymer	50 mg		30 mg	
	$T \pm \sigma_T$ (nm)	$R_{core} \pm \sigma_{core}$ (nm)	$T \pm \sigma_T$ (nm)	$R_{core} \pm \sigma_{core}$ (nm)
100% PLA-PEG	15.8 ± 4.1	56 ± 27	14.4 ± 4.0	56 ± 27
50% PLA-C_6H_{13} 50% PLA-PEG	18.6 ± 5.9	55 ± 27	17.1 ± 4.4	56 ± 28
50% PLA-C_3F_7 50% PLA-PEG	18.0 ± 5.8	54 ± 27	16.8 ± 4.4	56 ± 27
50% PLA-C_6F_{13} 50% PLA-PEG	18.0 ± 5.5	53 ± 27	14.2 ± 3.8	56 ± 28
50% PLA-C_8F_{17} 50% PLA-PEG	17.4 ± 4.9	54 ± 27	15.8 ± 4.0	57 ± 28
50% PLA-$C_{13}F_{27}$ 50% PLA-PEG	16.4 ± 4.8	53 ± 26	14.8 ± 3.5	56 ± 28

3-4- Cytotoxicity studies

The biological inertness of perfluorocarbons is well documented.[44] However, perfluorinated chains are often associated to toxicity due to their low excretion profiles and persistence in the organism, especially for linear perfluorinated chains longer than C_7F_{15}.[45-47] The influence of the perfluorinated end group on cellular viability was evaluated on two different cell lines, human umbilical vein endothelial (HUVEC) and murine macrophages (J774.A1) using an MTT assay. The nanocapsules were incubated at concentrations ranging from 0.01 to 10 mg/mL during 24h and 72h. At both incubation times, cell viability of HUVEC slightly decreases as nanocapsule concentration increases, but remains above 60% for all formulations even at high concentrations (Figure 7). Regarding J774.A1, after 24h incubation, cellular viability decreases down to 50% at 10 mg/mL, a huge concentration that is very unlikely to be reached in vivo. The viability decrease is even more pronounced after 72h incubation, with values reaching 20% cell viability at 10 mg/mL. The differences observed between the two cell lines can arise from the ability of J774.A1 macrophages to internalize faster and higher amounts of NCs than HUVEC.[48] For both cell types and both incubation time, within experimental error the fluorinated groups do not induce any specific toxicity in comparison to samples made from non-fluorinated polymers. However, additional cytotoxicity experiments after degradation of the polymers at 37°C are required to evaluate the possible toxicity

of the degradation products, as well as *in vivo* studies to study the effects arising from a prolonged exposure to NCs.

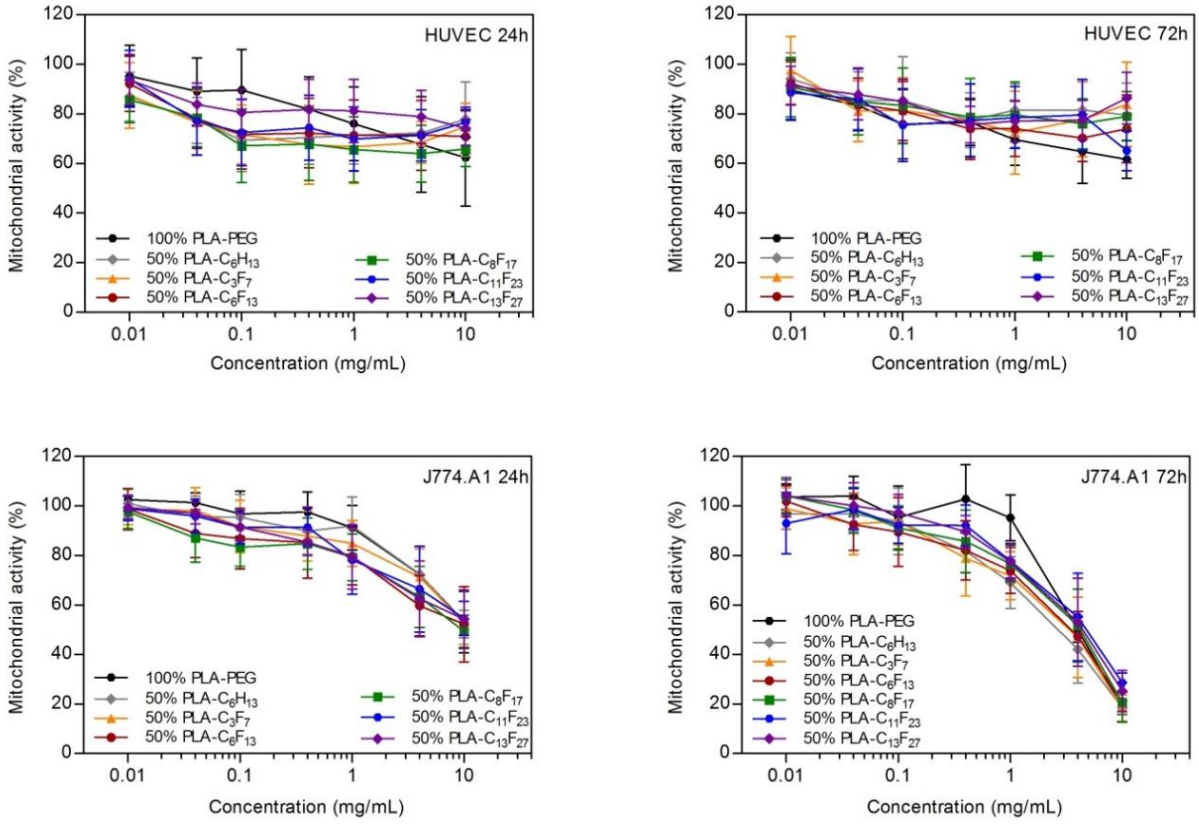

Figure 7: Viability assays on HUVEC (top) and J774.A1 (bottom) cell lines after 24h (left) and 72h (right) incubation with nanocapsules of increasing concentration. Results are presented as mean ± SD (n = 2)

3-5- *In vitro* ultrasound imaging

Although shell thickness was not significantly reduced, ultrasound imaging was performed on the two samples presenting the lowest thickness values to evaluate the potential impact of the fluorinated tail on the signal.

NCs made from 30 mg 50% PLA-C_6F_{13} 50% PLA-PEG and 100% PLA-PEG were therefore imaged *in vitro* at 37°C using ultrafast imaging[30] in fundamental mode. The backscattered intensity was 10 times higher with nanocapsules containing the fluorinated polymer (1.2 x 10^3 arbitrary units, a. u.) than with nanocapsules of pure PLA-PEG (0.1 x 10^3 a. u.) (Figure 8A). Given the similar thickness values (14.2 and 14.4 nm) of the two samples, the difference observed in the ultrasound response cannot originate from a difference of thickness. One possibility

could be the difference (1/2 lower) of percentage of PLA-PEG in the formulation. Indeed, Jablonowski et al. reported that adding PLA-PEG to PLA-shelled air microbubbles considerably reduces the echogenicity of the bubbles, in a dose-dependent manner.[49] However, the prime difference between the two types of NCs lies in the presence of the fluorine tail, which allows encapsulating more PFOB (encapsulation efficiency of 55%) than in pure PLA-PEG NCs (36%). Moreover, the scattering cross section of a particle is defined as $SCS = \frac{4\pi}{9} k^4 R^6 \left[\left(\frac{\kappa_d - \kappa}{\kappa}\right)^2 + \frac{3}{4}\frac{(\rho_d - \rho)^2}{(\rho_d + \rho)^2}\right]$ where k is the wavenumber, R is the radius of the particle, κ_d and κ the compressibilities of respectively the particle and the medium, ρ_d and ρ the densities of respectively the particle and the medium.[50] A contrast agent will therefore backscatter ultrasound waves more effectively if its radius is larger and if its physical properties (compressibility and density) differ a lot from the ones of the surrounding medium. Since the two samples have similar radii (58 and 62 nm), differences of compressibility and density of the NCs might also explain the difference of ultrasound contrast enhancement. Indeed, the high density of the fluorinated chain (density of corresponding fluorinated initiator is 1.6 $g.cm^{-3}$) increases the difference of density between the fluorinated NCs and surrounding water as compared to pure PLA-PEG NCs. The density of PEG 5000 g/mol is approximately 1.2 $g.cm^{-3}$ and it is 1.28 $g.cm^{-3}$ for PLGA.[51] To fully understand this echogenicity improvement in presence of fluorinated polymer, an exhaustive study is being carried as function of the fluorinated chain length and also by varying the ratio PLA-C_xF_y / PLA-PEG.

One can also observe that the backscattered intensity was much lower with NCs than with commercial Sonovue microbubbles (200 – 300 x 10^3 a.u.), that we used as control to allow a comparison using these particular set-up and ultrasound parameters (Figure 8). Since Sonovue microbubbles have a 20-fold larger radius than the formulated NCs and are filled with gaseous sulphur hexafluoride, achieving the same level of ultrasound contrast enhancement with liquid-filled nano-sized agents is, according to the formula above, difficult. Despite the lower echogenicity of fluorinated nanocapsules compared to microbubbles, they possess the potential to accumulate into the tumors by the EPR effect and induce ultrasound contrast enhancement to facilitate tumor diagnosis and characterization.[18, 20] This requires *in vivo* studies in the future.

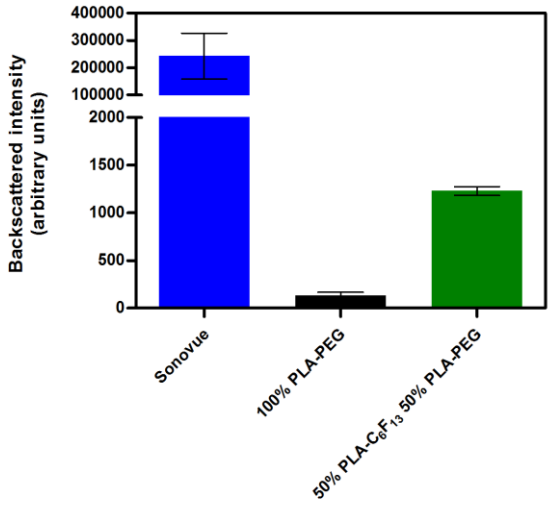

Figure 8 : Ultrasound backscattered intensity in fundamental mode for NCs made with low polymer amount (30 mg) and Sonovue microbubbles.

4- Conclusion

Perfluorinated end-capped polyesters with distinct perfluoroalkyl chain lengths were successfully synthesized and formulated into PEGylated nanocapsules of PFOB. These polymers do not induce any specific cytotoxicity compared to non-fluorinated PLAs. We demonstrate here that a linear fluorinated chain of length ranging from C_3F_7 to $C_{13}F_{27}$ at the extremity of a 20,000 g/mol PLA block does not significantly improve the wetting of the polymer layer at the PFOB/aqueous phase interface to allow reducing the thickness of the capsules containing 50% PLA-PEG, as previously observed with pure PLGA-PEG.[21] Despite similar thicknesses, fluorinated chains up to C_8F_{17} favor the increase of PFOB encapsulation efficiency. The combination of better PFOB encapsulation and an increase of nanocapsule shell density due to fluorination favors better ultrasound contrast enhancement of fluorinated nanocapsules compared to those obtained with pure PLA-PEG. Although this contrast enhancement was much lower than with commercial Sonovue microbubbles, these nano-sized capsules hold greater potential to accumulate into the tumors by the EPR effect and should allow tumor diagnosis.

5- Acknowledgements

Authors would like to thank Mehrez Sghaier and Najet Yagoubi from Laboratoire Matériaux et Santé (EA401, Univ. Paris-Sud) for DSC experiments and Stéphanie Denis (Institut Galien Paris-Sud) for her help with cell culture. This work has been supported by the Region Ile-de-France in the framework of DIM Nano-K. The present work has benefited also from the core facilities of Imagerie-Gif, (http://www.i2bc.paris-saclay.fr), member of IBiSA (http://www.ibisa.net), supported by “France-BioImaging” (ANR-10-INBS-04-01), and the Labex “Saclay Plant Science” (ANR-11-IDEX-0003-02). SANS analysis was performed using SasView software, originally developed by the DANSE project under NSF award DMR-0520547. Authors acknowledge financial support from ANR (Investissements d’Avenir, Nanobiotechnologies, ANR-10-NANO-06-04). Institut Galien Paris-Sud is a member of the Laboratory of Excellence LERMIT supported by a grant from ANR (ANR-10-LABX-33).

References

1. J. M. Correas, L. Bridal, A. Lesavre, A. Mejean, M. Claudon and O. Helenon, *Eur Radiol*, 2001, **11**, 1316-1328.
2. R. Diaz-Lopez, N. Tsapis and E. Fattal, *Pharm Res-Dordr*, 2010, **27**, 1-16.
3. V. Paefgen, D. Doleschel and F. Kiessling, *Front Pharmacol*, 2015, **6**.
4. M. Schneider, M. Arditi, M. B. Barrau, J. Brochot, A. Broillet, R. Ventrone and F. Yan, *Invest Radiol*, 1995, **30**, 451-457.
5. F. Yuan, M. Dellian, D. Fukumura, M. Leunig, D. A. Berk, V. P. Torchilin and R. K. Jain, *Cancer Res*, 1995, **55**, 3752-3756.
6. V. Leroy and T. Norisuye, *Chemphyschem*, 2016, **17**, 2787-2790.
7. E. G. Schutt, D. H. Klein, R. M. Mattrey and J. G. Riess, *Angew Chem Int Edit*, 2003, **42**, 3218-3235.
8. D. M. El-Sherif and M. A. Wheatley, *J Biomed Mater Res A*, 2003, **66A**, 347-355.
9. W. J. Cui, J. Z. Bei, S. G. Wang, G. Zhi, Y. Y. Zhao, X. S. Zhou, H. W. Zhang and Y. Xu, *J Biomed Mater Res B*, 2005, **73B**, 171-178.
10. C. Chlon, C. Guedon, B. Verhaagen, W. T. Shi, C. S. Hall, J. Lub and M. R. Bohmer, *Biomacromolecules*, 2009, **10**, 1025-1031.
11. Y. J. Zhao, W. X. Song, D. Wang, H. T. Ran, R. H. Wang, Y. Z. Yao, Z. G. Wang, Y. Y. Zheng and P. Li, *Acs Appl Mater Inter*, 2015, **7**, 14231-14242.
12. Z. B. Zha, J. R. Wang, S. H. Zhang, S. M. Wang, E. Qu, Y. Y. Zhang and Z. F. Dai, *Biomaterials*, 2014, **35**, 287-293.
13. P. Yang, D. Li, S. Jin, J. Ding, J. Guo, W. B. Shi and C. C. Wang, *Biomaterials*, 2014, **35**, 2079-2088.
14. M. M. Nestor, N. P. E. Kei, N. A. M. Guadalupe, M. E. S. Elisa, G. Q. Adriana and Q. G. David, *Ultrasonics*, 2011, **51**, 839-845.
15. V. Sanna, G. Pintus, P. Bandiera, R. Anedda, S. Punzoni, B. Sanna, V. Migaleddu, S. Uzzau and M. Sechi, *Mol Pharmaceut*, 2011, **8**, 748-757.
16. E. Pisani, N. Tsapis, J. Paris, V. Nicolas, L. Cattel and E. Fattal, *Langmuir*, 2006, **22**, 4397-4402.
17. E. Pisani, N. Tsapis, B. Galaz, M. Santin, R. Berti, N. Taulier, E. Kurtisovski, O. Lucidarme, M. Ourevitch, B. T. Doan, J. C. Beloeil, B. Gillet, W. Urbach, S. L. Bridal and E. Fattal, *Adv Funct Mater*, 2008, **18**, 2963-2971.
18. O. Diou, N. Tsapis, C. Giraudeau, J. Valette, C. Gueutin, F. Bourasset, S. Zanna, C. Vauthier and E. Fattal, *Biomaterials*, 2012, **33**, 5593-5602.
19. O. Diou, E. Fattal, V. Delplace, N. Mackiewicz, J. Nicolas, S. Meriaux, J. Valette, C. Robic and N. Tsapis, *Eur J Pharm Biopharm*, 2014, **87**, 170-177.
20. T. Boissenot, E. Fattal, A. Bordat, S. Houvenagel, J. Valette, H. Chacun, C. Gueutin and N. Tsapis, *Eur J Pharm Biopharm*, 2016, **108**, 136-144.
21. O. Diou, A. Brulet, G. Pehau-Arnaudet, E. Morvan, R. Berti, K. Astafyeva, N. Taulier, E. Fattal and N. Tsapis, *Colloids and surfaces. B, Biointerfaces*, 2016, **146**, 762-769.
22. J. G. Riess, *Tetrahedron*, 2002, **58**, 4113-4131.
23. M. P. Krafft and J. G. Riess, *Chem Rev*, 2009, **109**, 1714-1792.
24. M. A. Hillmyer and T. P. Lodge, *J Polym Sci Pol Chem*, 2002, **40**, 1-8.
25. W. K. Lee, I. Losito, J. A. Gardella and W. L. Hicks, *Macromolecules*, 2001, **34**, 3000-3006.
26. M. R. Bohmer, R. Schroeders, J. A. M. Steenbakkers, S. H. P. M. de Winter, P. A. Duineveld, J. Lub, W. P. M. Nijssen, J. A. Pikkemaat and H. R. Stapert, *Colloid Surface A*, 2006, **289**, 96-104.
27. T. J. Henderson, *Anal Chem*, 2002, **74**, 191-198.
28. A. Brulet, D. Lairez, A. Lapp and J. P. Cotton, *J Appl Crystallogr*, 2007, **40**, 165-177.
29. Sasview software, http://www.sasview.org, (accessed March 2016).
30. O. Couture, S. Bannouf, G. Montaldo, J. F. Aubry, M. Fink and M. Tanter, *Ultrasound Med Biol*, 2009, **35**, 1908-1916.
31. C. C. Chen, J. Y. Chueh, H. Tseng, H. M. Huang and S. Y. Lee, *Biomaterials*, 2003, **24**, 1167-1173.
32. E. Piorkowska, Z. Kulinski, A. Galeski and R. Masirek, *Polymer*, 2006, **47**, 7178-7188.
33. S. J. Park and S. H. Kim, *J Colloid Interf Sci*, 2004, **271**, 336-341.
34. O. Martin and L. Averous, *Polymer*, 2001, **42**, 6209-6219.

35. S. Essa, J. M. Rabanel and P. Hildgen, *Eur J Pharm Biopharm*, 2010, **75**, 96-106.
36. G. Giuntoli, L. Rosi, M. Frediani, B. Sacchi and P. Frediani, *J Appl Polym Sci*, 2012, **125**, 3125-3133.
37. A. Lucke, J. Tessmar, E. Schnell, G. Schmeer and A. Gopferich, *Biomaterials*, 2000, **21**, 2361-2370.
38. A. K. Salem, S. M. Cannizzaro, M. C. Davies, S. J. B. Tendler, C. J. Roberts, P. M. Williams and K. M. Shakesheff, *Biomacromolecules*, 2001, **2**, 575-580.
39. Y. Oda, R. Suzuki, T. Mori, H. Takahashi, H. Natsugari, D. Omata, J. Unga, H. Uruga, M. Sugii, S. Kawakami, Y. Higuchi, F. Yamashita, M. Hashida and K. Maruyama, *Int J Pharm*, 2015, **487**, 64-71.
40. H. Li, J. Wang, P. Wang, J. Zheng, F. Song, T. Yin, G. Zhou, R. Zheng and C. Zhang, *Chem Commun (Camb)*, 2014, **50**, 15163-15166.
41. Y. Koda, T. Terashima and M. Sawamoto, *Polym Chem-Uk*, 2015, **6**, 5663-5674.
42. A. Tressaud and G. Haufe, *Fluorine and Health: Molecular Imaging, Biomedical Materials and Pharmaceuticals*, 2008, DOI: Doi 10.1016/B978-0-444-53086-8.00020-5, Xi-Xiv.
43. F. De Jaeghere, E. Allemann, J. C. Leroux, W. Stevels, J. Feijen, E. Doelker and R. Gurny, *Pharm Res-Dordr*, 1999, **16**, 859-866.
44. M. P. Krafft and J. G. Riess, *J Polym Sci Pol Chem*, 2007, **45**, 1185-1198.
45. J. G. Riess, *Curr Opin Colloid In*, 2009, **14**, 294-304.
46. A. Zaggia and B. Ameduri, *Curr Opin Colloid In*, 2012, **17**, 188-195.
47. S. H. Barmentlo, J. M. Stel, M. van Doom, C. Eschauzier, P. de Voogt and M. H. S. Kraak, *Environ Pollut*, 2015, **198**, 47-53.
48. R. Reul, N. Tsapis, H. Hillaireau, L. Sancey, S. Mura, M. Recher, J. Nicolas, J. L. Coll and E. Fattal, *Polym Chem-Uk*, 2012, **3**, 694-702.
49. L. J. Jablonowski, D. Alfego, J. I. Andorko, J. R. Eisenbrey, N. Teraphongphom and M. A. Wheatley, *Biomaterials*, 2016, **103**, 197-206.
50. N. Dejong, F. J. Tencate, C. T. Lancee, J. R. T. C. Roelandt and N. Bom, *Ultrasonics*, 1991, **29**, 324-330.
51. K. Astafyeva, J. L. Thomas, F. Coulouvrat, M. Guedra, O. Diou, L. Mousnier, N. Tsapis, W. Urbach and N. Taulier, *Phys Chem Chem Phys*, 2015, **17**, 25483-25493.